ACS APPLIED MATERIALS & INTERFACES

Research Article

www.acsami.org

Peroxidase-Like Activity of Fe_3O_4@Carbon Nanoparticles Enhances Ascorbic Acid-Induced Oxidative Stress and Selective Damage to PC-3 Prostate Cancer Cells

Qiao An,[†,§] Chuanyu Sun,[‡,§] Dian Li,[†] Ke Xu,[*,‡] Jia Guo,[*,†] and Changchun Wang[†]

[†]State Key Laboratory of Molecular Engineering of Polymers, Department of Macromolecular Science, Fudan University, Shanghai 200433, P. R. China

[‡]Department of Urology, Huashan Hospital, Fudan University, Shanghai 200040, P. R. China

Supporting Information

ABSTRACT: Ascorbic acid (AA) is capable of inhibiting cancer cell growth by perturbing the normal redox state of cells and causing toxic effects through the generation of abundant reactive-oxygen species (ROS). However, the clinical utility of AA at a tolerable dosage is plagued by a relatively low in vivo efficacy. This study describes the development of a peroxidase-like composite nanoparticle for use in an AA-mediated therapeutic strategy. On the basis of a high-throughput, one-pot solvothermal approach, Fe_3O_4@C nanoparticles (NPs) were synthesized and then modified with folic acid (FA) on the surface. Particular focus is concentrated on the assessment of peroxidase-like catalytic activity by a chromogenic reaction in the presence of H_2O_2. The carbon shell of Fe_3O_4@C NPs contains partially graphitized carbon and thus facilitates electron transfer in the catalytic decomposition of H_2O_2, leading to the production of highly reactive hydroxyl radicals. Along with magnetic responsiveness and receptor-binding specificity, the intrinsic peroxidase-like catalytic activity of Fe_3O_4@C-FA NPs pronouncedly promotes AA-induced oxidative stress in cancer cells and optimizes the ROS-mediated antineoplastic efficacy of exogenous AA. In vitro experiments using human prostate cancer PC-3 cells demonstrate that Fe_3O_4@C-FA NPs serve as a peroxidase mimic to create hydroxyl radicals from endogenous H_2O_2 that is yielded in response to exogenous AA via an oxidative stress process. The usage of a dual agent leads to the enhanced cytotoxicity of PC-3 cells, and, because of the synergistic effect of NPs, the administrated dosage of AA is reduced markedly. However, because normal cells (HEK 293T cells) appear to have a higher capacity to cope with additionally generated ROS than cancer cells, the NP−AA combination shows little damage in this case, proving that selective killing of cancer cells could be achieved owing to preferential accumulation of ROS in cancer cells. A possible ROS-mediated mechanism is discussed to elucidate the pharmaceutical profile of the NP−AA agent. In general, this foundational study reveals that the peroxidase-like nanomaterials are applicable for modulating oxidative stress for the selective treatment of cancer cells by generating a high level of endogenous ROS.

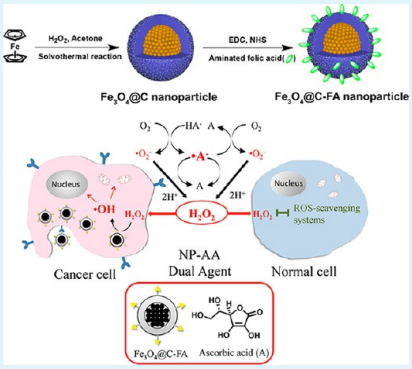

KEYWORDS: *ascorbic acid, magnetic nanoparticles, peroxidase, reactive oxygen species, target drug delivery, synergistic effect*

1. INTRODUCTION

Biochemistry mainly focuses on the understanding of information flow through biochemical signaling and energy flow through metabolism at the molecular level. Grounded in the findings of biochemistry, research on cancer treatments has witnessed a rapid development in recent years, resulting in improved therapeutic efficacy and selectivity as well as attenuated side effects and systematic toxicity.[1] As compared with the commonly used chemotherapy, biochemistry-based treatment adopts a mild therapeutic strategy to alter biochemical processes in cancer cells, such as oxidative stress, which generates reactive oxygen species (ROS) in aerobic organisms.[2] To our knowledge, once oxidative stress is activated vigorously, excessive ROS is yielded, causing oxidative damage to DNA, proteins, and lipids in the cancer cells.[3−5] However, as opposed to cancer cells, normal cells possess remarkable antioxidant capacity and thus tolerate a certain number of exogenous ROS stresses.[6] Therefore, this has resulted in the adoption of ROS-mediated treatment to establish biochemistry-based therapy for selectively killing cancer cells as well as for maintaining the viability of normal cells.[1,7,8]

Ascorbic acid (AA), which is an essential micronutrient commonly considered as an antioxidant,[9] has been used in cancer treatment for decades.[10−14] As reported, when pharmacological dosages of AA are administrated, cancer cells can be effectively damaged, but normal cells are not susceptible to it.[9,15] This selective treatment effect is ascribed to a pro-

Received: September 27, 2013
Accepted: November 7, 2013
Published: November 7, 2013

oxidative process in which AA triggers oxidative stress and impairs homeostasis in cellular redox cycling, resulting in the accumulation of ROS that cannot be tolerated in cancer cells.[16] As a complementary therapy, however, the high dosage of AA (4g/kg i.p. twice daily) is needed to achieve antitumor effects in mouse models, precluding its potential use in the clinic.[17] Therefore, reducing the dosages of AA without diminishing its anticancer activity has remained a persistent challenge. Although some accessory agents, including Mn(III)-porphyrin and 5-aminolevulinic acid,[17,18] have been able to show synergistic cytotoxicity against some cancer cells when used in combination with AA, the simultaneous delivery of dual agents to intended sites might pose one crucial issue, which is that they are most likely accumulated in different tissue regions, lowering their cooperative effect.

With this mind, we envisaged access to combine multifunctional inorganic nanoparticles (NPs) with AA to open up an innovative avenue in ROS-elevating-based therapy. To the best of our knowledge, a number of nanomaterials including ferromagnetic NPs,[19−21] graphene oxide,[22,23] carbon nanodots,[24] carbon nanotubes,[25] and gold NPs[26] have been found to possess intrinsic peroxidase-like activity, which can catalyze chromogenic reaction for use in the quantitative detection and sensing of chemicals in the presence of H_2O_2. In addition to their peroxidatic activity, however, the oxidase activity of peroxidases, which not only mediates the reduction of O_2 to superoxide and H_2O_2 but also catalyzes another type of reaction that results in the production of hydroxyl radicals ($^{\bullet}OH$) from H_2O_2 in the presence of superoxide under physiological conditions, is rarely considered.[27] Because $^{\bullet}OH$ radicals are extremely reactive and will attack most cellular components, peroxidases may be responsible for numerous destructive and toxic effects of activated oxygen. In view of the peroxidase-like characteristics of NPs, we speculated that NPs could also function as an oxidase to catalytically convert endogenous H_2O_2 to $^{\bullet}OH$ radicals, improving the ROS level in the cells. More importantly, multifunctional NPs with an accessibility for targeted delivery, optical labeling, and specific modification will significantly optimize ROS-mediated therapeutic efficacy.

Herein, we solvothermally synthesized a magnetic composite nanoparticle consisting of a magnetite nanoparticle-assembled cluster as the core and a carbon layer as the shell to which folic acid (FA) was applied to serve as a specific receptor to decorate the resulting composite NPs. The obtained core−shell-structured NPs (Fe_3O_4@C-FA) were equipped with multiple functions, including (1) peroxidase-like activity stemming from the carbon layer, (2) a rapid response to an applied magnetic field, and (3) FA-receptor targeting. Prior to its testing in a cell-based assay, the peroxidase-like activity of Fe_3O_4@C-FA NPs was evaluated through a model chromogenic reaction using horseradish peroxidase as a reference in which the amorphous carbon structure acted as a peroxidase mimic to mediate electron transfer between H_2O_2 and chromogenic substrates. Meanwhile, we demonstrated that Fe_3O_4@C-FA NPs catalyzed the conversion of H_2O_2 into $^{\bullet}OH$ radicals in a pH- and concentration-dependent manner, giving a high possibility that they could be used to elevate ROS level in cancer cells. To evaluate the synergistic cytotoxic effect of Fe_3O_4@C-FA NPs, human prostate cancer PC-3 cells were subjected to treatment by a combination of Fe_3O_4@C-FA NPs and AA. The results verified that the internalized Fe_3O_4@C-FA NPs remarkably promoted the ROS-mediated cytotoxicity of PC-3 cells even though a low dosage of AA was administered. In contrast, normal cells (HEK 293T) showed minimal cytotoxicity upon treatment by the same NP−AA combination. A possible ROS-mediated mechanism was then proposed to describe the change in the intracellular biochemical process as an attempt to interpret the origin of the synergistic cytotoxicity of Fe_3O_4@C-FA NPs when they are exposed to AA-induced oxidative stress.

2. EXPERIMENTAL SECTION

2.1. Materials. Ferrocene ($Fe(C_5H_5)_2$, 99%), ascorbic acid (99%), tetramethylbenzidine (98%), and *N*-(3-dimethylaminopropyl)-*N*-ethylcarbodiimide hydrochloride (EDC·HCl) were purchased from the Aladdin Chemical Reagent Co., Ltd. *N*-Hydroxysuccinimide (NHS) was purchased from Sigma-Aldrich Reagent Co., Ltd. Folic acid was purchased from Shanghai Chemical Reagent Co., Ltd. Hydrogen peroxide (H_2O_2, 30 wt %), acetone, and anhydrous ethanol were purchased from the Sinopharm Chemical Reagent Co., Ltd. All chemicals were used as received without further purification. The hydrogen peroxide assay kit was purchased from Beyotime Institute of Biotechnology Co., Ltd. The aminated folic acid was synthesized according to the literature.[28]

2.2. Synthesis of Fe_3O_4@Carbon Nanoparticles. A solvothermal method was adopted[29,30] and slightly modified to control the particle size to be around 100 nm. Briefly, ferrocene (0.15 g) was dissolved in 30 mL of acetone with the aid of ultrasonication for 10 min. H_2O_2 (0.5 mL) was slowly added, and then the mixture solution was magnetically stirred for 30 min. After that, the precursor solution was transferred into a Teflon-lined stainless autoclave with a capacity of 50 mL. The reaction was then maintained at 210 °C for 24 h and was then cooled to room temperature naturally. The mixture in the autoclave was subjected to ultrasonic treatment for 10 min. The precipitates were collected by a magnet from the mixture and washed with acetone three times.

2.3. Modification of Fe_3O_4@C NPs with Folic Acid. A mixture of EDC and NHS was added to a dispersion of Fe_3O_4@C NPs in water (5 mg mL^{-1}, 10 mL), and the solution was allowed to stand for 2.5 h before use. Then, 0.1 M borate buffer was used to adjust the pH to 8 to 9. The reaction was carried out with stirring overnight at room temperature after 4.8 mg of aminated folic acid dissolved in DMSO was added to the above solution. The product was isolated by a magnet and washed with water thoroughly.

2.4. Bioassay. Kinetic measurements were carried out in time-course mode by monitoring the absorbance change at 652 nm on a UV-3150 spectrometer (Shimadz, Japan). Experiments were carried out at 45 °C using 30 μg mL^{-1} of Fe_3O_4@C NPs in 0.5 mL of buffer solution (0.2 M NaOAc buffer, pH 3.0) with 800 mM TMB as substrate and 50 mM H_2O_2 unless otherwise stated. The Michaelis−Menten constant was calculated using the Lineweaver−Burk plot: $1/\nu = (K_m/V_{max})(C + 1/V_{max})$, where ν is the initial velocity, V_{max} is the maximal reaction velocity, and C is the concentration of substrate.[19,31]

2.5. Cell Viability. Cell viability was measured using the MTT method. A 200 μL volume of cells was seeded in a 96-well plate at a density of 4×10^3 cells per well followed by incubation for 24 h to allow their attachment. Different concentrations of Fe_3O_4@C-FA were added to the culture medium for 12 h. The medium was removed and rinsed once with medium, and then different concentrations of ascorbic acid diluted with 20 μL of MTT solution (5 mg mL^{-1} in PBS) were added for 1 h. The cells were then washed with PBS and incubated for an additional 6−48 h. MTT internalization was terminated by aspiration of the media, and the cells were lysed with 150 μL of DMSO. The absorbance of the suspension was measured at 570 nm. Cell viability was calculated using the following formula, where OD is the optical density:

$$\text{cell viability (\%)} = \frac{OD_{570(\text{sample})} - OD_{570(\text{blank})}}{OD_{570(\text{control})} - OD_{570(\text{blank})}} \times 100$$

2.6. Annexin V Staining Apoptosis Assay. Cell apoptosis rates were evaluated using an Annexin V-FITC apoptosis detection kit (Beyotime, China). After treatment with 20 μg mL^{-1} of Fe_3O_4@C-FA

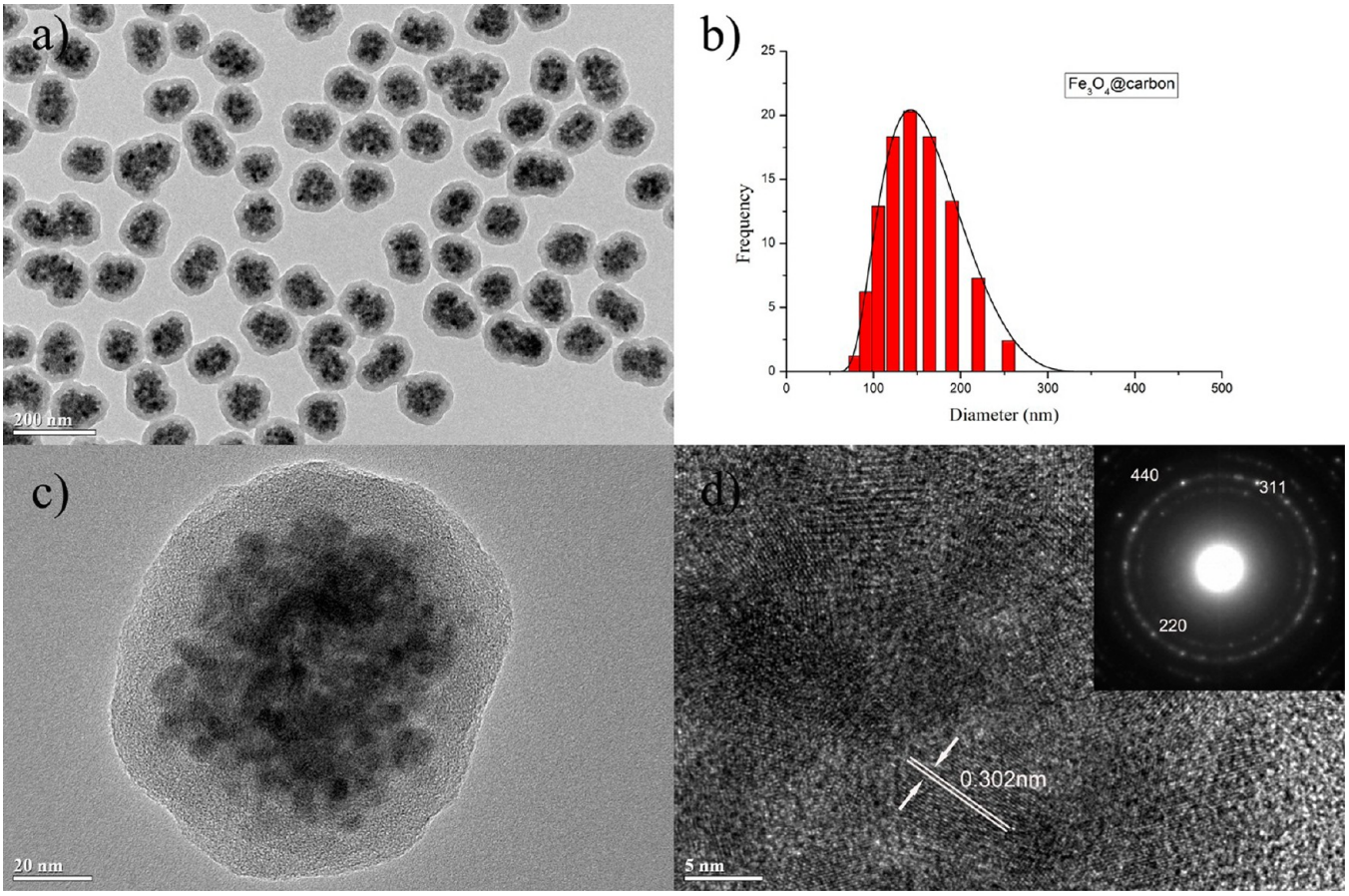

Figure 1. (a) TEM image of Fe_3O_4@C NPs, (b) hydrodynamic diameter distribution of Fe_3O_4@C NPs in water, (c) HR-TEM image of a representative single Fe_3O_4@C NP, and (d) lattice fringe and electron diffraction pattern of Fe_3O_4@C NPs (inset).

and/or 20 mM ascorbic acid for 48 h, the cells were harvested with 0.25% trypsin and resuspended in 100 μL of PBS to achieve a concentration of 1×10^6 mL^{-1}. Then, following the protocol of the manufacturer, 5 μL of Annexin V-FITC and 10 μL of PerCP-Cy5.5 (20 μg/mL) were added, and the cells were incubated in the dark for 15 min at room temperature. After the addition of 400 μL of the binding buffer, the stained cells were kept on ice and subjected to fluorescence-activated cell sorter analysis (FACS) using a FACScan flow cytometer (Becton-Dickinson, USA). The data was analyzed by CellQuest software (Becton-Dickinson, USA).

2.7. Western Blot Analysis. A total of 1×10^6 PC-3 cells incubated with Fe_3O_4@C-FA and ascorbic acid for 24 h were collected. After washing with cold PBS, the cytoplasmic fractions of the treated cells were subjected to 10% (w/v) sodium dodecyl sulfate-polyacrylamide gel electrophoresis (SDS-PAGE). The cytoplasm fractions of the PC-3 cells were prepared as follows. Control and treated cells were collected, washed with cold PBS, and suspended in 300 mL of buffer (210 mM D-mannitol, 70 mM sucrose, 5 mM EDTA, 10 mM HEPES-KOH, pH 7.4, 1 mg mL^{-1} each of aprotinin, pepstatin, and leupeptin, and 1 mM PMSF). The cells were homogenized and centrifuged at 700*g* for 7 min to remove nuclei and debris. The supernatant was centrifuged at 700*g* for 15 min followed by two further repetitions. The final pellet was saved as the fraction of isolated mitochondria. For cytoplasm fractions, the first 700*g* supernatant was centrifuged at 50 000*g* for 1 h at 4°C, and the supernatant was saved as the cytoplasm fractions. Following SDS-PAGE, western blot analysis was carried out to detect cytochrome c (cyt c) release using an anti-cyt c antibody.

2.8. Characterizations. HR TEM images were obtained on a JEM-2010 (JEOL, Japan) transmission electron microscope at an accelerating voltage of 200 kV. Powder X-ray diffraction (XRD) patterns were collected on a D8 advance (Bruker, Germany) diffraction meter with Cu Kα radiation at λ= 0.154 nm operating at 40 kV and 40 mA. Magnetic characterization was carried out on a Model 6000 physical-property measurement system (Quantum Design, USA) at 300 K. UV–vis spectra were measured on a UV-3150 (Shimadzu, Japan) ultraviolet–visible spectrophotometer. Fluorescence spectra were measured on a RF-5301PC (Shimadzu, Japan) fluorescence spectrophotometer. FTIR spectra were recorded on a Magna-550 (Nicolet, USA) spectrometer. Hydrodynamic diameter (D_h) and ζ-potential measurements were conducted with a Nano ZS Zetasizer (model ZEN3600, Malvern Instruments) using a He–Ne laser at a wavelength of 632.8 nm. Electron spin resonance (ESR) measurements were carried out at room temperature under the following conditions: microwave power, 20 mW; modulation amplitude, 1.0 G; modulation frequency, 100 kHz; receiver gain, 10^5; centre field, 3518 G; and sweep width, 100 G. A Bruker EMX spectrometer was used for all spectral acquisition. All samples were prepared in deionized water. DMPO (5,5-dimethyl-*N*-oxide pyrrolidone) was used to trap $^{\bullet}$OH to form the DMPO–OH spin adducts. Each Fe_3O_4@C NPs sample was mixed with DMPO in buffer, pH 7.4, and then H_2O_2 was added. Ethanol (2 vol %) was added to identify $^{\bullet}$OH radicals in a buffer of pH 4.0. Samples were prepared and transferred to a quartz capillary tube and placed in the ESR cavity. Each spectrum was recorded at 10 min for concentration-dependent changes; meanwhile, the effect of ethanol was evaluated by recording spectra at different times within 15 min. The Raman spectrum was recorded using a Renishaw spectrometer (model Invia Reflex) with 632.8 nm laser excitation. Nitrogen sorption measurements were performed at 77 K by an ASAP2020 volumetric adsorption analyzer (Micromeritics, USA). The samples were degassed at 150 °C for 12 h before measurement.

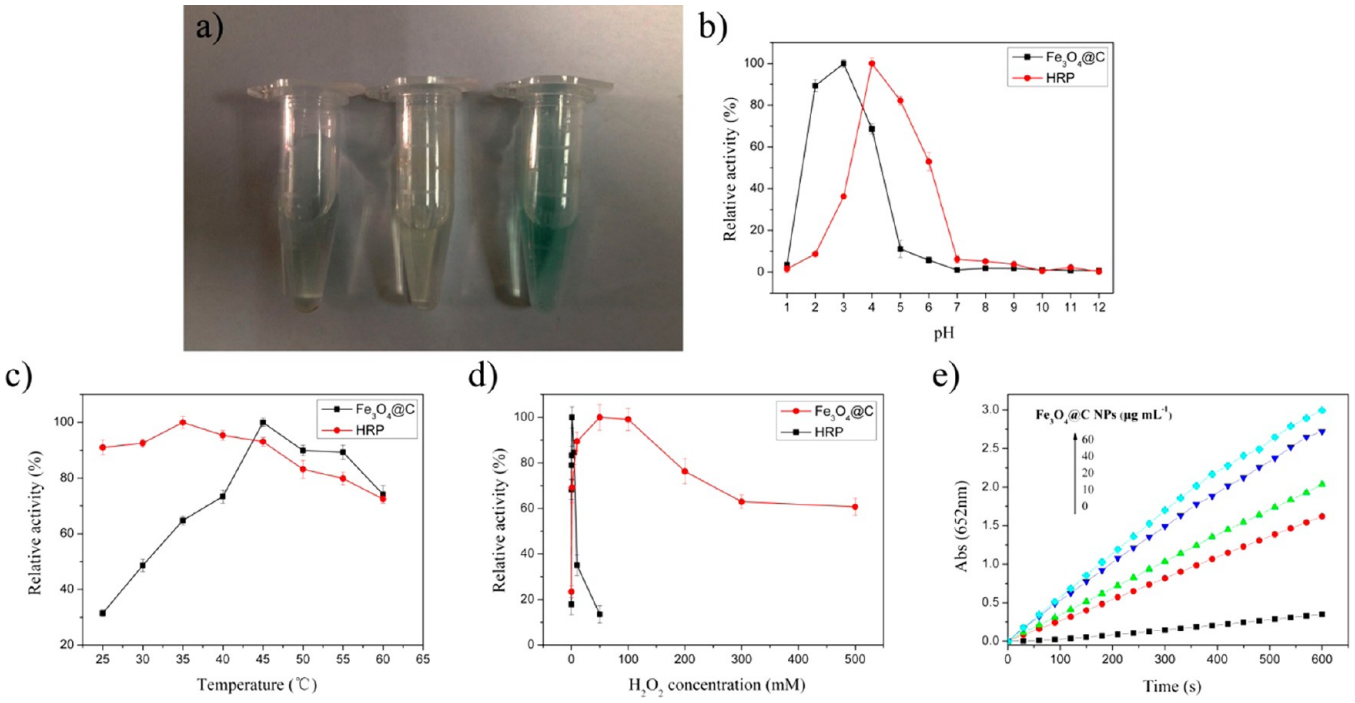

Figure 2. (a) Typical photographs for the chromogenic reaction of TMB catalyzed by Fe_3O_4@C NPs at pH 4.0 with H_2O_2. From left to right, 50 mM H_2O_2 and 800 μM TMB (colorless), 30 μg mL^{-1} of Fe_3O_4@C NPs (light yellow), and 50 mM H_2O_2, 800 μM TMB, and 30 μg mL^{-1} of Fe_3O_4@C NPs (turning blue). (b–d) Effects of pH (b), temperature (c), and H_2O_2 concentration (d) on catalytic activity of Fe_3O_4@C NPs (30 μg mL^{-1}) and HRP (1 ng mL^{-1}), respectively. (e) Time-dependent absorbance changes at 652 nm without or with addition of various concentrations of Fe_3O_4@C NPs at pH 3.0, 45 °C, and 50 mM H_2O_2.

3. RESULTS AND DISCUSSION

3.1. Synthesis and Characterization of Fe_3O_4@C NPs.

Fe_3O_4@Carbon nanoparticles (Fe_3O_4@C NPs) were synthesized in acetone with H_2O_2 as an oxidant and ferrocene as an iron precursor (Scheme S1 in the Supporting Information). As reported in our past work,[29,30] solvothermal conditions were used to improve the conversion of iron atoms to magnetite nanoparticles through the oxidation reaction of ferrocene with H_2O_2. The increasing number of magnetic nanoparticles then assembled into a larger colloidal nanocluster, which was tightly encapsulated by the graphitized carbon-based materials with abundant hydroxyl and carboxyl groups via coordination interaction. The resultant product was unambiguously analyzed by a series of characterizations. As displayed in Figure 1a, HR-TEM image of the obtained NPs show a diameter of roughly 120 nm, a narrow size distribution, and a definite core–shell structure. The hydrodynamic diameter (D_h) of composite NPs was evaluated by dynamic light scattering (DLS). The histogram in Figure 1b exhibits an average D_h of ca. 150 nm, indicating that the carbon shell renders NPs well-dispersed in water. The close observation of a representative NP in Figure 1c reveals a refined microstructure, wherein an amorphous polymer shell of 20 nm is entirely wrapped around the nanoparticle-attached cluster of 100 nm.

The crystalline structure in the core is shown in Figure 1d. The interplanar distance in the area of the lattice fringe is 0.30 nm, which is well in line with the distance of the (220) lattice planes of Fe_3O_4. In addition, one can see that the selected-area electron diffraction (SAED) pattern presents explicit diffraction rings and arcs, capable of being assigned to the typical (220), (311), and (440) reflections of Fe_3O_4, respectively. More substantial evidence for the formed NPs was provided by the powder X-ray diffraction pattern (Figure S1 in the Supporting Information). All of the diffraction peaks can correspond to the (220), (311), (222), (400), (422), (511), and (440) crystalline planes of cubic Fe_3O_4 (JCPDS 75-1609), validating the presence of Fe_3O_4 nanocrystals within the core–shell structure. The magnetization of Fe_3O_4@C NPs was assessed through the magnetic hysteresis loop measured by a vibrating sample magnetometer at 300 K (Figure S2 in the Supporting Information). Under an applied magnet field of below 20 000 Oe, the saturation magnetization reached 29 emu g^{-1} and the remanence (1.22 emu g^{-1}) and coercivity (31.07 Oe) both nearly approached the origin of the coordinates, indicative of the superparamagnetic characteristic of the encapsulated Fe_3O_4 nanocrystals.

The chemistry nature of the shell was characterized by FTIR spectrometry (Figure S3 in the Supporting Information). The characteristic bands at 1702 and 3408 cm^{-1} demonstrated the presence of abundant –COOH and –OH groups in the carbon layer. The peak at 1613 cm^{-1} could be attributed to C=C vibration, stemming from the inclusive aromatic groups in the carbon skeleton. Additionally, it was found that the Fe_3O_4@C NPs showed a zeta potential of –26.9 mV, demonstrating that the pendent carboxyl groups on the carbon shell were deprotonated to render the NPs negatively charged. The Raman spectrum of Fe_3O_4@C NPs (Figure S4 in the Supporting Information) showed the characteristic bands at 1580 and 1378 cm^{-1}, and they could be ascribed to the G and the D modes of carbon materials, respectively.[31] The G mode is derived from planar vibrations of sp^2 carbon atoms, and it is present in most graphite-like materials. The D mode originates from the structural defects relative to graphite. Thus, it can be determined that the carbon shell is amorphous and partially graphitized.

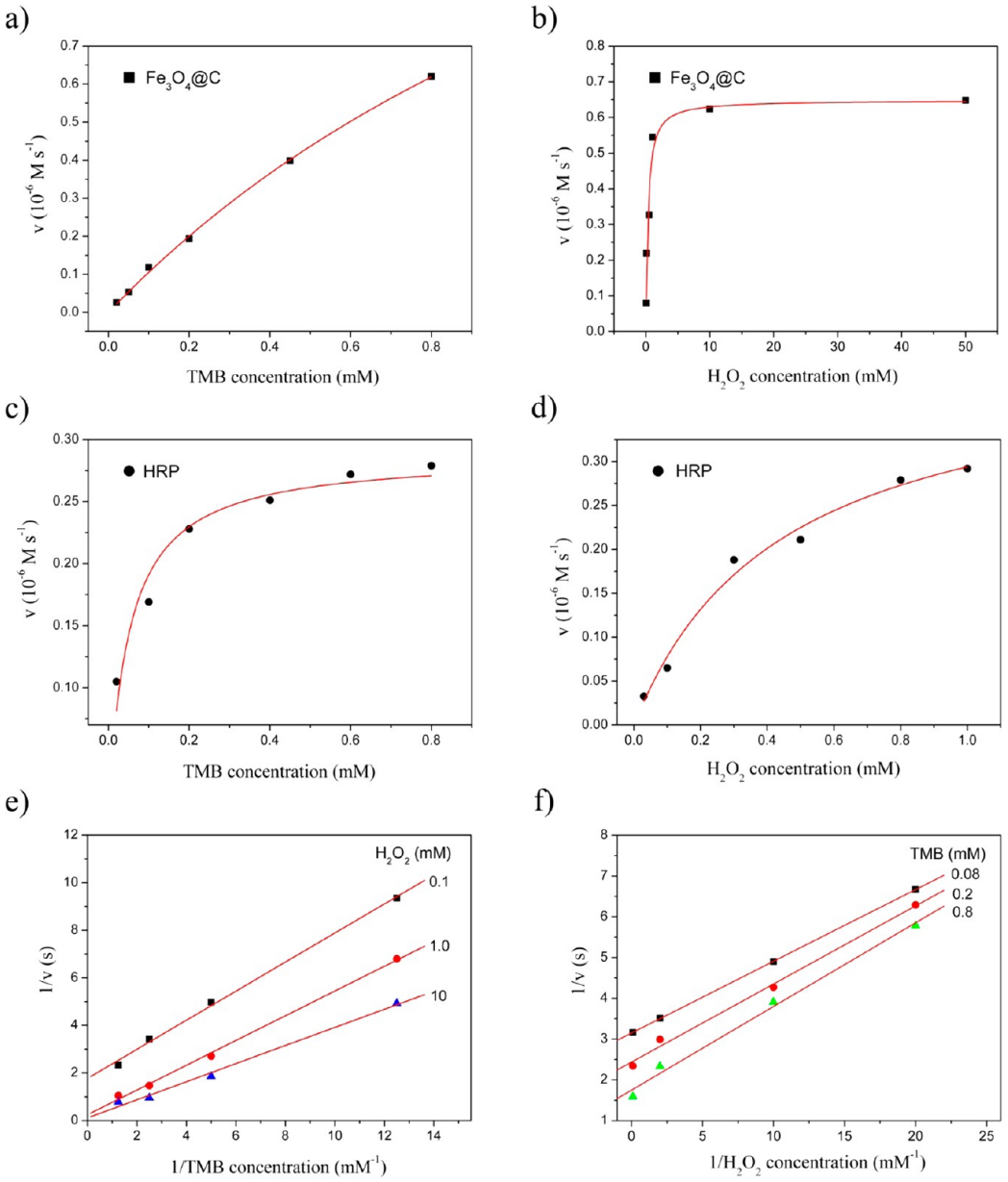

Figure 3. (a–d) Steady-state kinetic assay of peroxidase-like activity of Fe_3O_4@C NPs. The velocity of the reaction was measured using TMB and H_2O_2 as substrates, respectively, in 0.5 mL of NaAc buffer (0.2 M, pH 3.0) containing 30 μg mL^{-1} of Fe_3O_4@C at 45 °C (a, b) or in 0.5 mL of potassium acid phthalate buffer (0.2 M, pH 4.0) containing 0.5 ng of HRP at 35 °C (c,d). In panels a and c, the added H_2O_2 concentrations were 50 mM for Fe_3O_4@C NPs and 0.8 mM for HRP. In panels b and d, the added TMB concentration was 800 μM for both of the catalysts. (e, f) Double-reciprocal plots showing the effects of one substrate on the initial velocity as the other substrate was unchanged to understand the catalytic mechanism of Fe_3O_4@C NPs in the chromogenic reaction.

3.2. Peroxidase-Like Activity of Fe_3O_4@C NPs. Many kinds of carbon materials have intrinsic peroxidase-like activity owing to their graphite-like aromatic structures that prefer to mediate electron transfer and to enhance catalytic activity.[22−25] We speculated that the carbon shell that was proven to have partially graphitized carbons would also serve as peroxidase mimic to catalyze the reduction of H_2O_2. 3,3′,5,5′-Tetramethylbenzidine (TMB), a classic chromogenic reagent that is often used with peroxidase enzymes for the reduction of H_2O_2 to H_2O, was applied to examine the peroxidase-like activity of Fe_3O_4@C NPs. As shown in Figure 2a, the mixture solution in the presence of Fe_3O_4@C NPs appears blue upon addition of H_2O_2 and TMB together, indicating that Fe_3O_4@C NPs bear catalytic activity to oxidize TMB to the corresponding diimine by H_2O_2. Because this color change of TMB can be read on a UV−vis spectrometer at a wavelength of 652 nm (Figure S5 in the Supporting Information),[19] the catalytic activity of the Fe_3O_4@C NPs was estimated with use of horseradish peroxidase (HRP) as a reference and was further optimized under a wide scope of experimental conditions, including pH values, temperatures, and H_2O_2 concentrations. As displayed in Figure 2b−d, the best catalytic activity, comparable to that of HRP, could be obtained under the optimal conditions (i.e., pH 3.0, 45 °C, and 50 mM H_2O_2). The time-dependent absorbance changes against the used concentrations of Fe_3O_4@C NPs were then investigated. As is evident in Figure 2e, the absorbance at 652 nm was increased as the time was prolonged and the dosage of Fe_3O_4@C NPs was increased under the optimal

reaction conditions. One can see that 60 μg mL^{-1} of Fe_3O_4@C NPs allowed the reaction to achieve the maximum level and the largest rate in 10 min. Additionally, the color change could be halted by addition of sulfuric acid, as observed for the HRP-catalyzed reaction.[19] Because it is likely that the encapsulated Fe_3O_4 nanoparticles are etched by acid and the released Fe ions are involved in the chromogenic reaction, the porosity of the carbon shell was characterized by N_2 adsorption measurement at 77 K (Figure S6 in the Supporting Information). The results showed that the obtained carbon shell was nonporous and had a very low surface area (25.4 m^2 g^{-1}). This implies that the Fe_3O_4 nanoparticles are tightly covered by amorphous carbon and cannot take part in the color-change reaction of TMB.

To gain insight into the discrepancy in using Fe_3O_4@C NPs and HRP as catalysts for oxidation of TMB, the apparent steady-state kinetic parameters, namely, the maximum initial velocity (V_{max}) and Michaelis–Menten constant (K_m), were determined, respectively.[32] Because excessive H_2O_2 can inhibit the progress of the reaction, its concentration was limited to a certain range for Michaelis–Menten curves of two catalysts (Figures 3a–d). As listed in Table 1, the apparent K_m value of

Table 1. Kinetic Constants (K_m and V_{max}) of Fe_3O_4@C NPs and HRP Derived from Their Michaelis–Menten Curves in Figure 3a–d

catalyst	substrate	substrate fixed	K_m (mM)	V_{max} ($\times 10^{-8}$ M s^{-1})
Fe_3O_4@C	TMB	H_2O_2 (50 mM)	0.072	17.99
Fe_3O_4@C	H_2O_2	TMB (800 μM)	0.38	73.99
HRP	TMB	H_2O_2 (50 mM)	0.224	57.81
HRP	H_2O_2	TMB (800 μM)	0.25	29.97

Fe_3O_4@C NPs with H_2O_2 as the substrate is a little higher than that for HRP, agreeing well with the study that the maximal activity of Fe_3O_4@C NPs was acquired only when the H_2O_2 concentration was higher than that used for HRP. The apparent K_m value of the Fe_3O_4@C NPs with TMB as the substrate is approximately three times lower than that of HRP, implying that Fe_3O_4@C NPs have a higher affinity to TMB than HRP. In addition, we pursued the catalytic mechanism of Fe_3O_4@C NPs through the analysis of Lineweaver–Burk plots over a range of TMB and H_2O_2 concentrations. The results (Figure 3e,f) showed the double reciprocal plots of the initial velocity as a function of one substrate concentration while the second substrate concentration remained constant. The change in the trends of the initial velocity for H_2O_2 and TMB were both linear and paralleled each other, which is characteristic of a ping-pong mechanism, as observed for HRP.[19] This indicates that Fe_3O_4@C NPs bind and react with the first substrate and then release the product before reacting with the second substrate. Overall, we verified that Fe_3O_4@C NPs serve as a peroxidase mimic to mediate electron communication between substrates to result in the reductive cleavage of H_2O_2. Additionally, their outstanding catalytic activity allows for an alternative option to eliminate harsh reaction conditions and to manipulate the oxidative stress processes for ROS-mediated therapeutic use.

3.3. Production of Hydroxyl Radicals Catalyzed by Fe_3O_4@C NPs. Peroxidases constitute a class of heme-containing enzymes that typically catalyze the dehydrogenation of phenolic and endiolic substrates in the presence of H_2O_2 and are often regarded as antioxidant enzymes, protecting cells from the destructive influence of ROS. However, in addition to this peroxidatic activity, peroxidases possess an oxidase activity that causes the production of $^{\bullet}$OH from H_2O_2 in the presence of superoxide through the biological Haber–Weiss reaction. There is evidence that the toxicity of ROS strongly depends on the presence of Fenton catalysts such as iron ions or peroxidases if the ROS concentration exceeds the capacity of the ROS-scavenging reaction.[27] Therefore, it was proposed that Fe_3O_4@C NPs might act as a peroxidase mimic, giving rise to destructive and oxidative damage to cancer cells. As above mentioned, because Fe_3O_4 nanoparticles are entrapped within the nonporous carbon matrix, the oxidase activity of the composite materials will be attributed to the partially graphitized carbons, which is advantageous for mediating electron transfer in the catalysis reaction. Electron spin resonance (ESR), a reliable spectroscopic technique that tracks the unpaired electron present in a free radical,[33] was applied to examine radical production through the use of Fe_3O_4@C NPs. 5,5-Dimethyl-pyrroline *N*-oxide (DMPO) was used as spin trap to detect the short-lived $^{\bullet}$OH radicals in the form of spin adduct, DMPO–OH, a relatively stable paramagnetic chemical with a characteristic ESR signal of a 1:2:2:1 quartet.[34] As shown in Figure 4a, with increasing concentrations of Fe_3O_4@C NPs, the ESR signal intensity for the generated $^{\bullet}$OH radicals is correspondingly increased in the presence of 5 mM H_2O_2 at pH 7.4. This implies that Fe_3O_4@C NPs are capable of the catalytic conversion of H_2O_2 to $^{\bullet}$OH radicals in a concentration-dependent manner. As a control, H_2O_2 added alone shows a relatively low population of $^{\bullet}$OH radicals. In addition, the ESR measurement of Fe_3O_4@C NPs at pH 4.0 was acquired for the assessment of catalytic activity. In this case, ethanol, an efficient scavenger of $^{\bullet}$OH radicals, was used together with DMPO to unambiguously identify the generation of $^{\bullet}$OH radicals because the side reaction is present in the formation of the DMPO–OH spin adduct without a source of $^{\bullet}$OH radicals.[35] The findings from Figure 4b reveal that the DMPO–OH signal intensity is dependent on the added concentrations of Fe_3O_4@C NPs at pH 4.0; moreover, compared with those obtained at pH 7.4, the stronger characteristic peaks assigned to the DMPO–OH adduct is observed when 20 μg mL^{-1} of Fe_3O_4@C NPs was used for decomposition of 5 mM H_2O_2 under otherwise identical conditions. This reveals that the catalytic performance of Fe_3O_4@C NPs is preferably activated in acid medium. In addition to the signals from the DMPO–OH adduct, a set of new peaks emerged upon addition of ethanol. As shown in Figure 4c, because ethanol trapped $^{\bullet}$OH radicals to form $^{\bullet}CHCH_3OH$ radicals, the characteristic signals can be assigned to a new DMPO adduct with $^{\bullet}CHCH_3OH$ radicals.[36] With prolonged time, the DMPO–$CHCH_3OH$ adduct was unstable and inclined to decompose to the DMPO–OH adduct with an increase in signal intensity. Again, the results confirm that Fe_3O_4@C NPs mimic peroxidase to yield reactive $^{\bullet}$OH radicals when exposed in H_2O_2, promising a great potential for their use in a ROS-elevating therapeutic strategy.

3.4. ROS-Mediated Apoptosis of PC-3 Cells using AA-NP Couple. Prior to the study of anticancer activity from a combination of Fe_3O_4@C NPs and AA, Fe_3O_4@C NPs were subjected to surface modification by folic acid for improving their affinity to cancer cells with the overexpressed folate receptors.[37,38] Specifically, the aminated folic acid (FA-NH_2), confirmed by FTIR measurement (Figure S3c in the Supporting Information), was grafted onto Fe_3O_4@C NPs by the amidation reaction of the ended amine groups on FA-NH_2

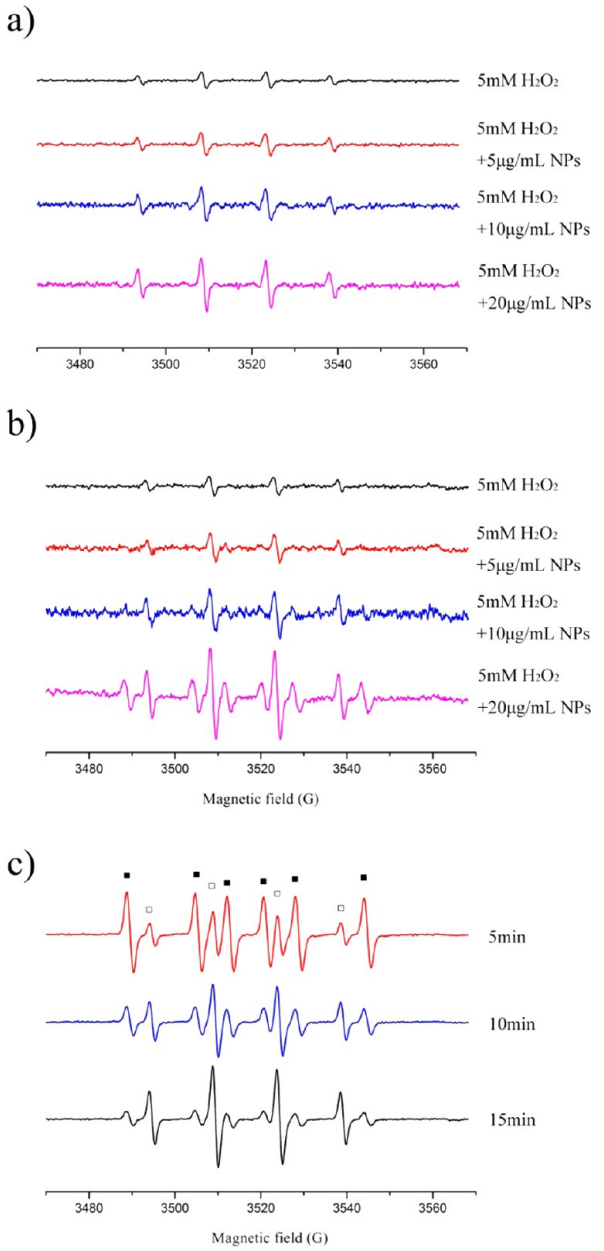

Figure 4. (a) ESR spectra of the •OH radical spin adduct of DMPO produced in 50 mM of PBS buffer (pH 7.4) containing 20 mM DMPO, 5 mM H_2O_2, and different concentrations of Fe_3O_4@C NPs. (b) ESR spectra of the •OH radical spin adduct of DMPO produced in 50 mM HAc-NaAc buffer (pH 4.0) with 2% ethanol containing 20 mM DMPO, 5 mM H_2O_2, and different concentrations of Fe_3O_4@C NPs. (c) Time-dependent ESR spectra recorded in 50 mM HAc-NaAc buffer (pH 4.0) with 2% ethanol containing 20 mM DMPO, 5 mM H_2O_2, and 20 μg mL^{-1} of Fe_3O_4@C NPs.

and the carboxylate groups on the surface of the Fe_3O_4@C NPs. The formed Fe_3O_4@C-FA conjugates were characterized by various spectroscopy technologies. Because of the grafted FA on Fe_3O_4@C NPs, the fluorescence emission spectrum showed the typical emission peak at 450 nm (Figure S7a in the Supporting Information), the UV−vis spectrum exhibited a new broad absorbance at 353 nm (Figure S7b in the Supporting Information), and the FTIR spectrum involved a characteristic band of CO−NH groups at 1248 cm^{-1}, indicating that amide bonds formed between FA and Fe_3O_4@C NPs (Figure S3a in the Supporting Information).

The PC-3 human prostate cancer cell line was applied to assess the cytotoxicity of H_2O_2, AA, and Fe_3O_4@C-FA NPs alone or in combination using an MTT assay. As a control, the effect of Fe_3O_4@C-FA NPs on the cytostatic activity of exogenous H_2O_2 was investigated first in PC-3 cells. Before MTT assay, the culture medium for PC-3 cells was incubated for 12 h in the presence of a certain dosage of Fe_3O_4@C-FA NPs; in turn, H_2O_2 was added, and the mixture was incubated for 1 h, washed with fresh culture medium, and then incubated for another 18 h. As depicted in Figure 5a, although the used dosages of Fe_3O_4@C-FA NPs were varied in the range of 2.5−20 μg mL^{-1}, the damage to PC-3 cells was negligible when NPs were used alone. When PC-3 cells were incubated with 15 or 30 μM H_2O_2 in the presence of Fe_3O_4@C-FA NPs, the cell viability pronouncedly declined in a concentration-dependent manner, and the trend mainly relies on the dosage of H_2O_2 rather than Fe_3O_4@C-FA NPs. Following the above finding, AA-induced apoptosis of PC-3 cells was studied to examine the efficacy of endogenous H_2O_2 produced by oxidative stress. The concentration of endogenous H_2O_2 could be determined by a hydrogen peroxide assay kit. As seen in Figure 5b, 0.5 and 2 mM AA are able to generate endogenous H_2O_2 with concentrations of 11 and 33 μM, respectively. Thus, instead of exogenous H_2O_2, 0.5 and 2 mM of AA were used in the study of cell viability. As shown in Figure 5c, these dosages of AA cannot remarkably harm the PC-3 cells, leading to ca. 75% of cell viability if they are used without Fe_3O_4@C-FA NPs. This implies that endogenous H_2O_2 is presumably eliminated through multiple metabolism pathways. Under otherwise identical conditions, when 2.5 μg mL^{-1} of Fe_3O_4@C-FA NPs were cultivated in PC-3 with 2 mM AA, the cell viability was dramatically decreased to 50%, less than that obtained without the addition of Fe_3O_4@C-FA NPs (75%). Although 0.5 mM AA did not achieve an equal efficacy for killing PC-3 cells, a successive increase in the concentration of the NPs induced distinctive cytotoxicity, ultimately leading to 40% cell apoptosis. In addition, time-dependent cell death was also studied when 20 μg mL^{-1} of Fe_3O_4@C-FA NPs were combined with 0.5 or 2 mM of AA for the treatment of PC-3 cells (Figure 5d). It can be seen that the cytotoxicity was notably enhanced with the extended incubation time; roughly 75% cell death was eventually observed after 48 h. These findings clarify that Fe_3O_4@C-FA NPs do function as a peroxidase mimic to enhance the generation of highly toxic radicals when exposed to conditions of AA-induced oxidative stress, leading to a increasing inhibition of PC-3 cells in a dosage- and time-dependent manner.

We investigated the apoptosis mechanism of PC-3 cells when treated with Fe_3O_4@C-FA and/or AA by flow cytometry. Figure 6 shows the distributions of cell populations after a 48 h incubation of PC-3 cells using NPs, AA, and NP−AA combination, respectively. A dot-plot Annexin V-FITC versus PerCP-Cy5.5 is separated into four clusters: viable cells (lower-left quadrant), early apoptotic cells (lower-right quadrant), necrotic or late apoptotic cells (phase consecutive to apoptosis in vitro, upper-right quadrant), and necrotic cells (upper-left quadrant). It can be seen that significant differences induced by NPs, AA, or the NP−AA combination relative to the control were found in the early apoptosis region. Of these, the NP−AA combination resulted in 49.1% of early apoptotic cells, higher than those obtained using Fe_3O_4@C-FA (4.9%) and AA

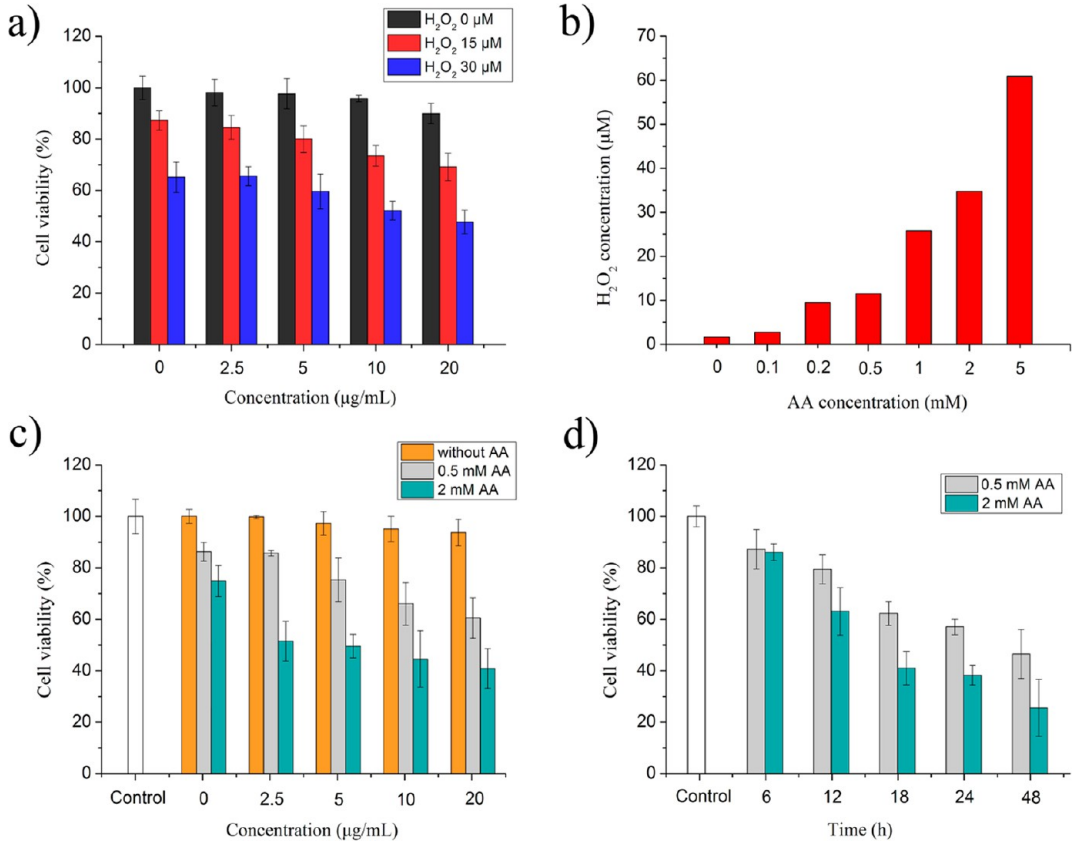

Figure 5. (a) Effects of Fe_3O_4@C-FA NPs on PC-3 cell viability in the presence of different concentrations of H_2O_2. (b) Evaluation of endogenous H_2O_2 in PC-3 cells induced by various doses of AA using a hydrogen peroxide assay kit. (c) Effects of the concentration of Fe_3O_4@C-FA NPs on PC-3 cell viability with treatment of 0.5 and 2 mM of AA, respectively. (d) Time-dependent effects of 20 μg mL^{-1} of Fe_3O_4@C-FA NPs on PC-3 cell viability with treatment of 0.5 and 2 mM of AA, respectively. Prior to detection by MTT assay, the cells were incubated with a certain dose of Fe_3O_4@C-FA NPs for 12 h and then treated with AA for 1 h, washed, and cultured for another 18 h.

(33.2%) alone. Again, the complementary effectiveness of Fe_3O_4@C-FA NPs and AA was well-demonstrated and primarily resulted in early apoptosis during cell death.

To gain insight into the induction of apoptosis using this dual agent, a consecutive study was conducted to determine whether the level of oxidative stress was changed in this process. The mitochondria plays a key role in apoptosis through diverse signaling pathways,[39] and oxidative-stress-induced apoptosis is often accompanied by mitochondrial membrane rupture and the release of cytochrome c (cyt c),[40,41] which is a well-known downstream signal molecule triggering caspase-dependent apoptosis. As a result, the current oxidative stress model can be defined by confirming the cyt c pathway. In this context, the subcellular distribution of cyt c was investigated from cytoplasmic fractions of PC-3 cells. As shown in Figure 7, the results from the western blot imply that the cyt c content is markedly increased in the cytoplasmic fraction when Fe_3O_4@C-FA NPs and AA were used in combination for 24 h. This indicates that severe damage occurs in the mitochondria and that the oxidative stress is activated gradually.

To evaluate the specificity of the dual agent, the human embryonic kidney (HEK) 293T cell line (normal cells) was treated by an identical procedure and evaluated by the MTT assay. In Figure 8, one can see that when Fe_3O_4@C-FA NPs and AA were used alone they both show negligible cytotoxicity irrespective of the administered dosages. When they were used together, about 20% cytotoxicity to HEK 293T cells was observed. Because normal cells have the ability to eliminate excess ROS by ROS-scavenging systems, the inhibitory impact of the dual agent on HEK 297T cell growth and proliferation is not significant.

Taken together, this study demonstrates that a combination of Fe_3O_4@C-FA NPs and AA show synergistic effects on killing cancer cells, whereas it results in little damage to normal cells. We propose a possible mechanism to interpret this process in Figure 9. The exogenous AA causes oxidative stress that disturbs the normal redox state of the cells and thus influences cytotoxicity because the endogenous H_2O_2 is beyond the scavenging capacity of the cells. However, the cytotoxic response of cancer cells will only emerge if the quantity of endogenous H_2O_2 remains at a high level. As a result, the use of a therapeutic chaperone is likely to reduce the administered dosage of AA. Grounded in the above results and findings, the peroxidase-like activity of Fe_3O_4@C-FA NPs facilitates conversion of H_2O_2 to highly toxic $^{\bullet}OH$ radials to damage organelles in cancer cells severely. On the contrary, the cytotoxicity induced by the same level of endogenous H_2O_2 in normal cells is lower than that in the cancer cells. The reason for this is not only because normal cells possess relatively strong ROS-scavenging systems but also because the lower catalytic activity of Fe_3O_4@C-FA NPs is shown in a neutral environment.

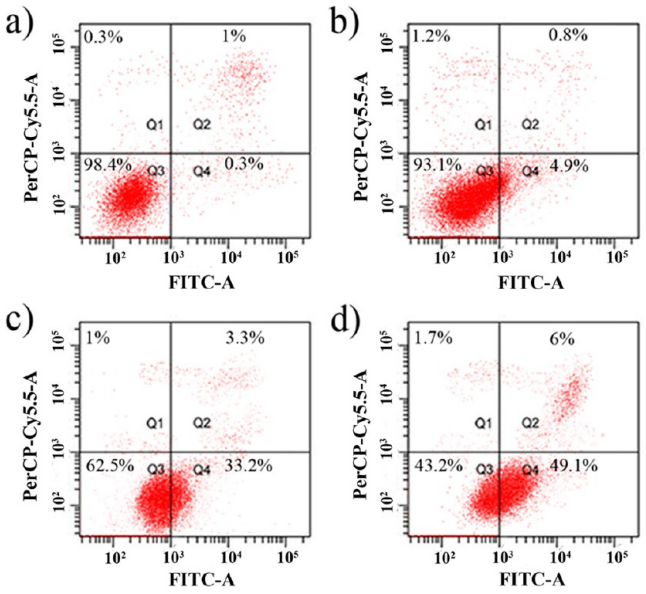

Figure 6. FACS analysis of apoptosis and necrosis of PC-3 cells stained by annexin V-FITC and PerCP-Cy5.5 in the presence of Fe_3O_4@C-FA and/or AA. In each plot, the lower-left quadrant represents viable cells, the upper-left quadrant represents necrotic cells, the lower-right quadrant represents early apoptotic cells, and the upper-right quadrant represents necrotic or late apoptotic cells. (a) Control, (b) cells treated with Fe_3O_4@C-FA NPs for 12 h and then incubated for 48 h, (c) cells exposed to AA for 1 h and then incubated for another 48 h, and (d) cells treated with Fe_3O_4@C-FA NPs for 12 h and AA for 1 h and then incubated for another 48 h.

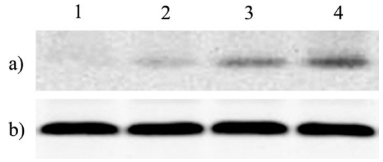

Figure 7. Western blot analysis of the oxidative-stress-mediated release of cyt c after PC-3 cells were treated with Fe_3O_4@C-FA NPs and AA. (a) Cyt c in cytoplasm fractions and (b) actin control. Lane 1, control; lane 2, treated with Fe_3O_4@C-FA for 12 h; lane 3, treated with Fe_3O_4@C-FA for 12 h and AA for 1 h and then incubated for another 18 h; and lane 4, treated with Fe_3O_4@C-FA for 12 h and AA for 1 h and then incubated for another 24 h.

4. CONCLUSIONS

We developed an interesting ROS-mediated therapeutic strategy in which endogenous H_2O_2 triggered by AA in the oxidative stress process is converted into $^{\bullet}OH$ radials through the catalysis mediated by Fe_3O_4@C-FA NPs, resulting in enhanced cytotoxicity against cancer cells. The intrinsic peroxidase-like activity of Fe_3O_4@C-FA NPs was verified by the model chromogenic reaction with HRP as a reference in which the carbon shell containing moderate amounts of graphitized carbon is conducive to mediating electron transfer and thus to enhancing the catalytic oxidation of the substrate TMB in the presence of H_2O_2 to produce color change. In addition, it is ascertained that the produced $^{\bullet}OH$ radials are dependent on the concentration of Fe_3O_4@C-FA NPs and can reach a maximum level at pH 4.0. The apoptosis of PC-3 cells (human prostate cancer cell line) was studied to demonstrate the synergistic cytotoxicity of a combination of Fe_3O_4@C-FA NPs and AA in which Fe_3O_4@C-FA NPs serve as a peroxidase

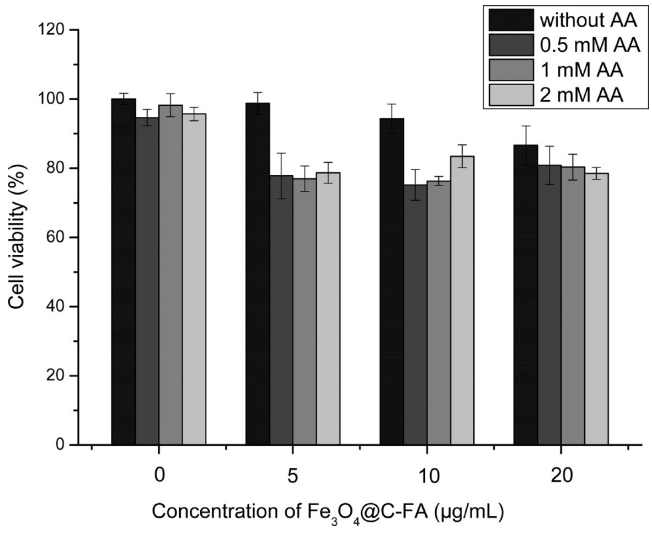

Figure 8. Estimation of HEK 293T cell viability by MTT assay upon treatment with different concentrations of Fe_3O_4@C-FA NPs and AA.

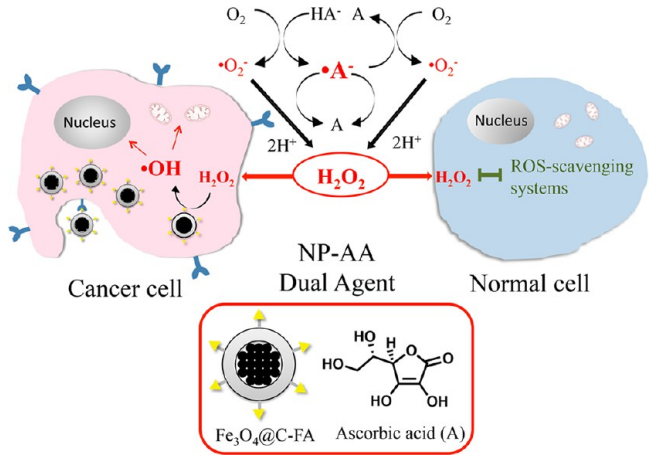

Figure 9. Schematic illustration of the oxidative-stress-induced cytotoxicity to different cells using a combination of Fe_3O_4@C-FA NPs and AA. For the cancer cells, the exogenous AA results in an increasing level of endogenous H_2O_2 and causes cytotoxicity with the assistance of Fe_3O_4@C-FA NPs. The process starts from the production of endogenous H_2O_2 that is involved in (1) electron transfer from O_2 to AA, producing $^{\bullet}A^-$ and $^{\bullet}O_2^-$ and (2) reoxidation of $^{\bullet}A^-$ to A with O_2 forming $^{\bullet}O_2^-$, wherein H_2O_2 would be eventually produced in both cases. Then, Fe_3O_4@C-FA NPs act as peroxidase mimic to create highly toxic $^{\bullet}OH$ radicals through the catalytic decomposition of endogenous H_2O_2. For normal cells, the oxidative stress reaction is largely suppressed because of their strong ROS-scavenging systems.

mimic to encourage the creation of toxic radicals like Fenton's reagent. Even though a mild oxidative stress is triggered by a low dosage of AA, the ROS-mediated anticancer efficacy is significantly enhanced with the assistance of Fe_3O_4@C-FA NPs, in sharp contrast to the case when AA is used alone. Moreover, relatively little damage to normal cells implies that the NP−AA combination is able to selectively kill cancer cells. Combined with the multiple functions of the NPs, it is most likely that targeted delivery of NPs will further optimize ROS-mediated therapeutic potency at specific sites. Taking all of this into account, we believe that the biomimetic characteristic of nanomaterials will open up an innovative route toward the

dx.doi.org/10.1021/am4042367 | ACS Appl. Mater. Interfaces 2013, 5, 13248−13257

development of ROS-mediated therapeutic strategies for use in cancer treatment.

■ ASSOCIATED CONTENT

Supporting Information

Schematic illustration of the preparation of Fe_3O_4@C-FA nanoparticles as well as their PXRD pattern, magnetic hysteresis curve, FTIR spectra, UV−vis spectra, fluorescence emission spectra, N_2 adsorption−desorption isotherm, and Raman spectrum. This material is available free of charge via the Internet at http://pubs.acs.org.

■ AUTHOR INFORMATION

Corresponding Authors

* E-mail: huashanxuke@163.com (K.X.).
* E-mail: guojia@fudan.edu.cn (J.G.).

Author Contributions

[§]These authors contributed equally to this work.

Notes

The authors declare no competing financial interest.

■ ACKNOWLEDGMENTS

This work was supported by the National Science Foundation of China (grant nos. 21004012 and 81372756), the Health Bureau of Shanghai Municipality (2008113 and XYQ2011028), the Doctoral Fund of the Ministry of Education of China (grant no. 20100071120007), the Scientific Research Foundation for Returned Scholars of the Ministry of Education of China, and the research fund of the Key Laboratory for Advanced Technology in Environmental Protection of Jiangsu Province.

■ REFERENCES

(1) Trachootham, D.; Alexandre, J.; Huang, P. *Nat. Rev. Drug Discovery* **2009**, *8*, 579−591.
(2) Zhou, Q.; Liu, L. Z.; Fu, B.; Hu, X.; Shi, X.; Fang, J.; Jiang, B. H. *Carcinogenesis* **2007**, *28*, 28−37.
(3) Perry, G.; Raina, A. K.; Nunomura, A.; Wataya, T.; Sayre, L. M.; Smith, M. A. *Free Radical Biol. Med.* **2000**, *28*, 831−834.
(4) Beckman, K. B. *J. Biol. Chem.* **1997**, *272*, 19633−19636.
(5) Berlett, B. S. *J. Biol. Chem.* **1997**, *272*, 20313−20316.
(6) Peer, D.; Karp, J. M.; Hong, S.; Farokhzad, O. C.; Margalit, R.; Langer, R. *Nat. Nanotechnol.* **2007**, *2*, 751−760.
(7) Schumacker, P. T. *Cancer Cell* **2006**, *10*, 175−176.
(8) Raj, L.; Ide, T.; Gurkar, A. U.; Foley, M.; Schenone, M.; Li, X.; Tolliday, N. J.; Golub, T. R.; Carr, S. A.; Shamji, A. F.; Stern, A. M.; Mandinova, A.; Schreiber, S. L.; Lee, S. W. *Nature* **2011**, *475*, 231−234.
(9) Chen, Q.; Espey, M. G.; Sun, A. Y.; Pooput, C.; Kirk, K. L.; Krishna, M. C.; Khosh, D. B.; Drisko, J.; Levine, M. *Proc. Natl. Acad. Sci. U.S.A.* **2008**, *105*, 11105−11109.
(10) Jorissen, W. P.; Belinfante, A. H. *Science* **1934**, *79*, 13.
(11) Mc, C. W. *Arch. Pediatr.* **1954**, *71*, 313−322.
(12) Cameron, E.; Pauling, L. *Proc. Natl. Acad. Sci. U.S.A.* **1976**, *73*, 3685−3689.
(13) Cameron, E.; Pauling, L. *Proc. Natl. Acad. Sci. U.S.A.* **1978**, *75*, 4538−4542.
(14) Padayatty, S. J.; Riordan, H. D.; Hewitt, S. M.; Katz, A.; Hoffer, L. J.; Levine, M. *Can. Med. Assoc. J.* **2006**, *174*, 937−942.
(15) Chen, Q.; Espey, M. G.; Krishna, M. C.; Mitchell, J. B.; Corpe, C. P.; Buettner, G. R.; Shacter, E.; Levine, M. *Proc. Natl. Acad. Sci. U.S.A.* **2005**, *102*, 13604−13609.
(16) Chen, P.; Stone, J.; Sullivan, G.; Drisko, J. A.; Chen, Q. *Free Radical Biol. Med.* **2011**, *51*, 681−687.
(17) Tian, J.; Peehl, D. M.; Knox, S. J. *Cancer Biother. Radiopharm.* **2010**, *25*, 439−448.
(18) Frank, J.; Flaccus, A.; Schwarz, C.; Lambert, C.; Biesalski, H. K. *Free Radical Biol. Med.* **2006**, *40*, 827−836.
(19) Gao, L.; Zhuang, J.; Nie, L.; Zhang, J.; Zhang, Y.; Gu, N.; Wang, T.; Feng, J.; Yang, D.; Perrett, S.; Yan, X. *Nat. Nanotechnol.* **2007**, *2*, 577−583.
(20) Chen, Z.; Yin, J. J.; Zhou, Y. T.; Zhang, Y.; Song, L.; Song, M.; Hu, S.; Gu, N. *ACS Nano* **2012**, *6*, 4001−4012.
(21) Guan, G.; Yang, L.; Mei, Q.; Zhang, K.; Zhang, Z.; Han, M. Y. *Anal. Chem.* **2012**, *84*, 9492−9497.
(22) Song, Y.; Qu, K.; Zhao, C.; Ren, J.; Qu, X. *Adv. Mater.* **2010**, *22*, 2206−2210.
(23) Guo, Y.; Deng, L.; Li, J.; Guo, S.; Wang, E.; Dong, S. *ACS Nano* **2011**, *5*, 1282−1290.
(24) Shi, W.; Wang, Q.; Long, Y.; Cheng, Z.; Chen, S.; Zheng, H.; Huang, Y. *Chem. Commun.* **2011**, *47*, 6695−6697.
(25) Song, Y.; Wang, X.; Zhao, C.; Qu, K.; Ren, J.; Qu, X. *Chem.—Eur. J.* **2010**, *16*, 3617−3621.
(26) Jv, Y.; Li, B.; Cao, R. *Chem. Commun.* **2010**, *46*, 8017−8019.
(27) Chen, S. X.; Schopfer, P. *Eur. J. Biochem.* **1999**, *260*, 726−735.
(28) Li, K.; Pan, J.; Feng, S.-S.; Wu, A. W.; Pu, K.-Y.; Liu, Y.; Liu, B. *Adv. Funct. Mater.* **2009**, *19*, 3535−3542.
(29) An, Q.; Yu, M.; Zhang, Y. T.; Ma, W. F.; Guo, J.; Wang, C. C. *J. Phys. Chem. C* **2012**, *116*, 22432−22440.
(30) An, Q.; Zhang, P.; Li, J. M.; Ma, W. F.; Guo, J.; Hu, J.; Wang, C. C. *Nanoscale* **2012**, *4*, 5210−5216.
(31) Ferrari, A. C.; Robertson, J. *Phys. Rev. B* **2000**, *16*, 14059−14107.
(32) Peng, Y.; Li, X.; Ren, J.; Qu, X. *Chem. Commun.* **2007**, 5176−5178.
(33) Rana, S.; Chawla, R.; Kumar, R.; Singh, S.; Zheleva, A.; Dimitrova, Y.; Gadjeva, V.; Arora, R.; Sultana, S.; Sharma, R. K. *J. Pharm. BioAllied Sci.* **2010**, *2*, 80−87.
(34) Vander Borght, T.; Labar, D.; Pauwels, S.; Lambotte, L. *Int. J. Radiat. Appl. Instrum., Part A* **1991**, *42*, 103−104.
(35) Lemercier, J. N.; Squadrito, G. L.; Pryor, W. A. *Arch. Biochem. Biophys.* **1995**, *321*, 31−39.
(36) Fang, G. D.; Zhou, D. M.; Dionysiou, D. D. *J. Hazard. Mater.* **2013**, *250-251*, 68−75.
(37) Low, P. S.; Henne, W. A.; Doorneweerd, D. D. *Acc. Chem. Res.* **2008**, *41*, 120−129.
(38) Sudimack, J.; Lee, R. J. *Adv. Drug Delivery Rev.* **2000**, *41*, 147−162.
(39) Lu, M.; Gong, X. *Cell Biol. Int.* **2009**, *33*, 658−664.
(40) Richter, C.; Gogvadze, V.; Laffranchi, R.; Schlapbach, R.; Schweizer, M.; Suter, M.; Walter, P.; Yaffee, M. *Biochim. Biophys. Acta* **1995**, *1271*, 67−74.
(41) Jurgensmeier, J. M.; Xie, Z.; Deveraux, Q.; Ellerby, L.; Bredesen, D.; Reed, J. C. *Proc. Natl. Acad. Sci. U.S.A.* **1998**, *95*, 4997−5002.